Ultrasonics 54 (2014) 343–350

Contents lists available at SciVerse ScienceDirect

Ultrasonics

journal homepage: www.elsevier.com/locate/ultras

Elastic–plastic cube model for ultrasonic friction reduction via Poisson's effect

Sheng Dong, Marcelo J. Dapino *

Smart Vehicle Concepts Center, Department of Mechanical and Aerospace Engineering, The Ohio State University, Columbus, OH 43210, United States

ARTICLE INFO

Article history:
Received 12 January 2013
Received in revised form 9 May 2013
Accepted 24 May 2013
Available online 4 June 2013

Keywords:
Ultrasonic lubrication
Friction reduction
Piezoelectric actuators

ABSTRACT

Ultrasonic friction reduction has been studied experimentally and theoretically. This paper presents a new elastic–plastic cube model which can be applied to various ultrasonic lubrication cases. A cube is used to represent all the contacting asperities of two surfaces. Friction force is considered as the product of the tangential contact stiffness and the deformation of the cube. Ultrasonic vibrations are projected onto three orthogonal directions, separately changing contact parameters and deformations. Hence, the overall change of friction forces. Experiments are conducted to examine ultrasonic friction reduction using different materials under normal loads that vary from 40 N to 240 N. Ultrasonic vibrations are generated both in longitudinal and vertical (out-of-plane) directions by way of the Poisson effect. The tests show up to 60% friction reduction; model simulations describe the trends observed experimentally.

1. Introduction

Dynamic friction exists at the interface of two surfaces in contact that move relative to each other. Ultrasonic vibrations, usually generated by a piezoelectric stack, can reduce friction when they are superimposed onto the macroscopic velocity. Friction force can be controlled between high and low by modulating vibration velocity, which is done by applying various voltages to the stack.

The earliest studies in ultrasonic lubrication were conducted by Mason [1] to reduce wear in relays, and were further investigated by Pohlman and Lehfeldt [2]. Since then, many studies have been done. Ultrasonic vibrations of different frequencies have been applied in various ways onto the sliding surfaces, as shown in Fig. 1. Usually, ultrasonic vibrations are applied to only one of the two surfaces. Littmann et al. [3,4] used a 60 kHz piezoelectric actuator sliding on a guide track. As shown in pattern 1, the applied vibration is parallel to the relative sliding direction.

Kumar [5] conducted tests applying vibrations longitudinal and transverse to the macroscopic direction, shown in patterns 1 and 2. It was concluded that longitudinal vibrations are more effective at reducing friction than transverse vibrations and that velocity ratio greatly influences friction reduction. Popov et al. [6] investigated the influence of out-of-plane ultrasonic vibrations (pattern 3) employing different material combinations. It was discovered that ultrasonic vibrations create less friction reduction on soft materials than on hard materials. It was also argued that the contact stiffness between materials affects the degree of friction reduction. Dong and Dapino [7] successfully generated vibrations conjugating patterns 1 and 3 using the Poisson effect and experimentally investigated friction reduction with various normal loads, contact metals and global stiffness.

Comprehensive modeling of systems equipped with ultrasonic lubrication devices necessitates precise models for ultrasonic lubrication. In addition to experimental studies on ultrasonic lubrication, analytical models have been proposed. Littman et al. [3,4] presented a relationship between velocity ratio and friction ratio. Popov et al. [6] established a relationship between friction reduction and vibration amplitudes under various normal loads. Bharadwaj and Dapino [8,9] studied the dependence of friction reduction on macroscopic sliding velocity, normal load, contact stiffness, and global stiffness.

Unlike traditional lubrication, ultrasonic lubrication is solid state and requires no oil or grease. Therefore, it is of great interest for manufacturing operations and vehicle applications. Many conventional metal forming processes such as wire drawing, forging, rolling, and extrusion have been or are being investigated for use under ultrasonic lubrication [10]. Pasierb and Wojnar [13] experimentally investigated the effectiveness of high frequency (16 kHz) vibrations in deep drawing of thin walled product using a laboratory scale testing apparatus. They found that "active friction" triggers when the velocity of ultrasonic vibration is larger than the velocity of the deforming sheet, and it could significantly reduce the forming load. Ashida and Aoyama [14] applied 21 kHz ultrasonic vibration to a small scale (30 mm diameter) round cup drawing die and found that local ultrasonic vibration at the die shoulder radius was more effective than vibrating the entire die. Cunefare et al. [11,12] used 20 kHz dither generated by a

* Corresponding author. Tel.: +1 (614) 688 3689.
E-mail address: dapino.1@osu.edu (M.J. Dapino).

0041-624X/$ - see front matter © 2013 Elsevier B.V. All rights reserved.
http://dx.doi.org/10.1016/j.ultras.2013.05.011

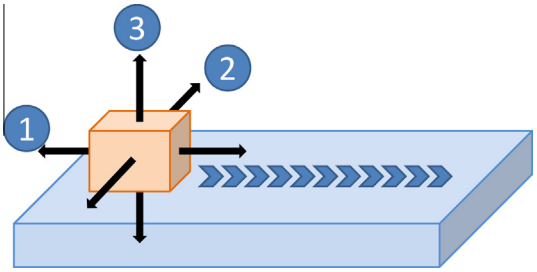

Fig. 1. Ways to apply ultrasonic vibrations.

piezoceramic rod inside the caliper piston to reduce the frictional squeal in braking systems. It was shown that the squeal decreases as the amplitude of vibrations increases, and the noise can be totally eliminated when the amplitude reaches a threshold value.

The effect of high frequency (15 kHz) vibration was investigated in the wire drawing process by Hayashi et al. [15] with the radial direction vibration being found more effective than axial direction vibration in reducing the forming load. In addition, the ultrasonic vibration effect was diminished as the drawing speed increased to more than 1 m/s. Ultrasonic vibration at 20 kHz was applied to the blanking process by Hatanaka et al. [16] in 2003 and was simulated by Yeh et al. [17] in 2011. The quality of sheared edge profile was significantly improved, and the punch load was reduced by applying ultrasonic vibration in the blanking process. A non-linear friction model was developed using a strip pull test and was applied to a square cup drawing simulation.

Dong and Dapino [7] first examined ultrasonic lubrication at a microscopic level by using an elastic cube model, which takes the following parameters into consideration: normal forces, contact parameters, and ultrasonic vibration amplitudes. This model offers good simulation, matching with test results under small normal loads, but discrepancies appear under bigger normal loads. This paper improves the cube model by introducing plasticity to the contact parameters calculation; a new equation is formulated to calculate microscopic deformation, and friction integration over half of the vibration period is added to calculate friction reduction.

2. Ultrasonic lubrication cube model

Nominal flat surfaces have asperities [18], as shown in Fig. 2. Physical contact between two surfaces takes place on asperities so that the actual contact area is much smaller than the nominal contact area. This paper utilizes the concept that a cube model is used to represent asperities in contact. As shown in Fig. 3, the area of the top surface of the cube is equal to the real area of two surfaces in contact, which is denoted as A_r. The height of the cube is equal to the distance between the two surfaces, which is denoted d.

The cube model consists of three parts: contact, friction and friction reduction. The contact model examines the contact of two surfaces from the level of asperities and calculates the contact

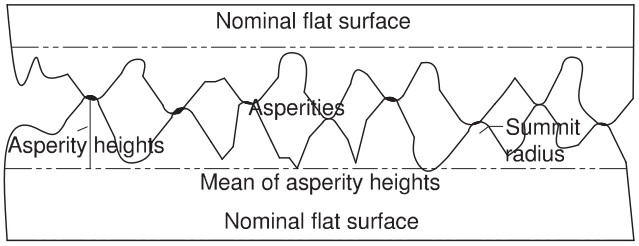

Fig. 2. Contacts of asperities between two nominal flat surfaces.

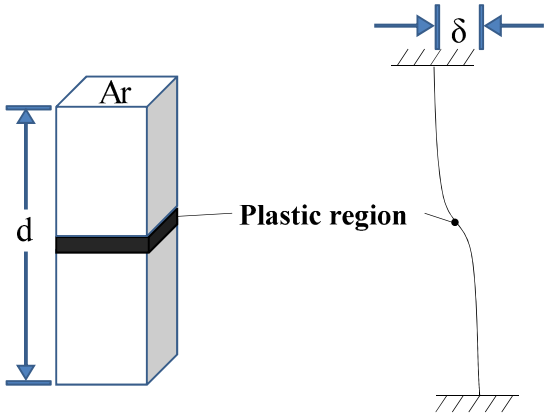

Fig. 3. Cube model and its deformation.

parameters. The friction model examines the relationship between friction force and deformation of contacting asperities. The friction reduction model describes how ultrasonic vibrations change the contact parameters and microscopic deformations, and therefore, the friction force.

2.1. Contact model

This paper employs assumptions widely adopted in surface contact studies [19]. The contact between two rough surfaces can be replaced by one rough surface contacting a smooth surface. Surfaces in contact are assumed isotropic. No bulk deformation is taken into consideration, but bulk displacement is examined when ultrasonic vibrations are applied. Asperity peaks have a spherical shape with a uniform radius R_s.

First asperity contacts form when two surfaces contact each other with normal force applied. These contacts remain elastic only under very special conditions, such as very smooth surfaces with asperities having even heights or under very low normal loads [20]. In more common cases, where asperities are uneven and normal loads are high, the first asperity contacts exhibit plastic deformations and new pairs of asperities come into contact until normal loads are balanced. By analyzing the contact of a single asperity pair, a critical interference ω_c is used to determine whether the asperity contact is elastic or plastic [21]

$$\omega_c = \left[\frac{C_v \pi (1-v^2) Y_0}{2E^*}\right]^2 R_s, \tag{1}$$

where C_v is a hardness coefficient related to the Poisson's ratio of the softer material ($C_v = 1.234 + 1.256v$), v is the Poisson's ratio, Y_0 is the failure strength of the softer material, R_s is the average radius of asperity summits, and E^* is the combined Young's modulus of two materials ($1/E^* = (1-v_1^2)/E_1 + (1-v_2^2)/E_2$). When the height of an asperity is smaller than ω_c, the contact is elastic, otherwise it is plastic.

The heights of the asperities follow a Gaussian distribution. An exponential probability distribution ϕ is used instead of a Gaussian distribution [21]

$$\phi(z) = ce^{-\lambda z}, \tag{2}$$

where z is the normalized distance between the asperity summit and the mean of asperity heights, and c and λ are constants. It was shown in [21] that when c and λ are equal to 17 and 3, respectively, the exponential distribution best approximates a Gaussian distribution, while being simpler to implement.

When two surfaces slide relative to each other through a tangential force, contacting asperity pairs deform longitudinally as a

whole until the bonds are broken. Plastically deformed asperities may come off from the main body if weak bonds exist in the asperities rather than at the interfaces. This is one of the explanations for wear. New asperity contacts take place as old ones are separated during sliding. Overall, there are always sufficient asperities in contact to balance the normal force. Meanwhile, the tangential force that permits sliding to continue is balanced by the deformations of the asperity contacts. This tangential force is considered as the overall dynamic friction force.

Total normal force F_n is the summation of elastic and plastic contributions [22],

$$F_n = F_e + F_p. \tag{3}$$

Following the method in [21], the total normal force from the elastically deformed asperities is an integral of the normal force of asperity contact pairs over the range of asperity heights, from the lowest to the critical interference. The integral has a closed form solution,

$$F_e = \frac{4c\beta(R_q/R_s)^{1/2}}{3\lambda^{5/2}}\left[\frac{3\sqrt{\pi}}{4}\mathrm{erf}\left(\sqrt{\lambda\omega_c/R_q}\right) - \frac{(\lambda\omega_c/R_q)^{3/2} + \frac{3}{2}\sqrt{\lambda\omega_c/R_q}}{e^{\lambda\omega_c/R_q}}\right]e^{-\lambda d/R_q}, \tag{4}$$

where β is the roughness parameter ($\beta = \eta R_q R_s$), η is the areal density of asperities, R_q is the standard deviation of surface roughness, and erf is the error function used to get the closed form solution ($\mathrm{erf}(x) = \frac{2}{\sqrt{\pi}}\int_0^x e^{-t^2}dt$).

Similarly, the total normal force from the plastically deformed asperities is calculated as

$$F_p = \frac{c\pi\beta C_v(1-\nu^2)Y_0}{E^*\lambda^2}\left(2 + \lambda\frac{\omega_c}{R_q}\right)e^{-\lambda(d+\omega_c)/R_q}. \tag{5}$$

It is noted that F_e, F_p, and F_n are functions of d. The cube height d corresponding to a normal load F_n can be calculated from (3)–(5).

The actual contact area A_r is calculated as

$$A_r = A_e + A_p. \tag{6}$$

The actual contact area of the elastically deformed asperities is

$$A_e = \frac{c\pi\beta A_n}{\lambda^2}\left[1 - \left(1 + \lambda\frac{\omega_c}{R_q}\right)e^{\lambda\omega_c/R_q}\right]e^{-\lambda d/R_q}, \tag{7}$$

where A_n is the nominal contact area. The actual contact area of the plastically deformed asperities is

$$A_p = \frac{c\pi\beta A_n}{\lambda^2}\left(2 + \lambda\frac{\omega_c}{R_q}\right)e^{-\lambda(d+\omega_c)/R_q}. \tag{8}$$

2.2. Friction model

The cube deforms when two surfaces slide relative to each other. Since asperities are connected to the body of the material, it can be assumed that two ends of the cube are fixed and the cube itself can be treated like a bending beam, as shown in Fig. 3. The plastic region works as a plastic hinge (it provides no higher moment when its maximum moment is reached). The tangential contact stiffness K_t can be derived from the bending stiffness of a beam with two fixed ends [23]. Given the geometry of the cube, K_t has the form

$$K_t = \frac{E^* A_r^2}{d^3}. \tag{9}$$

Friction has been studied extensively [24]. Many friction models have been proposed, and this paper adopts Dahl's model. Dahl [25] supplies an ordinary differential equation to calculate time-dependent microscopic deformation δ as

$$\frac{d\delta}{dt} = v_{rel}\left[1 - \frac{K_t\delta}{F_{t0}}\mathrm{sgn}(v_{rel})\right], \tag{10}$$

where v_{rel} is the relative sliding velocity between two surfaces, which is equal to 5 mm/s in this paper, and F_{t0} is the static friction between two surfaces measured from experiments.

Dynamic friction is calculated as the product of microscopic deformation and tangential contact stiffness,

$$F_t = K_t\delta. \tag{11}$$

2.3. Friction reduction model

As described in the introduction, ultrasonic vibrations can be applied in different ways. Vibrations can be projected in three orthogonal directions: in-plane parallel, in-plane perpendicular, and out-of-plane perpendicular to the sliding direction, denoted as u, v, and w, respectively. The deformations are functions of coordinates x, y, z, and time t. For δ, d, A_r, and K_t, prime symbols are employed to denote changed parameters after the application of ultrasonic vibrations.

It is assumed in the cube model that projection w has little influence on friction reduction and the projection u is directly added to the longitudinal microscopic deformation δ. Hence, in the presence of ultrasonic vibrations, the new deformation (denoted δ') is the sum of the initial deformation and the longitudinal projection of the vibrations,

$$\delta' = \delta + u. \tag{12}$$

The out-of-plane perpendicular projection v changes distance between two surfaces, which is equal to the height of the cube. The new cube height when ultrasonic vibrations are applied is

$$d' = d + v. \tag{13}$$

The actual contact area changes with the new distance and its value A_r' can be calculated using 6, 7 and 8. Therefore, the new tangential contact stiffness K_t' is calculated as

$$K_t' = \frac{E^* A_r'^2}{d'^3} = \frac{E^* A_r'^2}{(d+v)^3}. \tag{14}$$

Vibrations add relative vertical movements between two surfaces. When the surfaces move towards each other, friction increases so that the sliding pauses. The two surfaces are now in stick phase. When two surfaces move away from each other, friction is reduced and the sliding resumes, defined as slip phase. The sliding process consists of stick and slip phases alternating at an ultrasonic frequency. The overall dynamic friction is the average friction at the slip phase.

Assuming that each slip and stick phase takes place in half of one ultrasonic vibration period, T, the overall dynamic friction is the integral of the time-dependent friction over the slip phase,

$$F_t' = \frac{2}{T}\int_0^{T/2} K_t'\delta' dt = \frac{2}{T}\int_0^{T/2} \frac{E^* A_r'^2(\delta + u)}{(d+v)^3} dt. \tag{15}$$

Note that the parameters K_t', A_r', u, v, d', and δ' are time-dependent. This friction is considered as reduced friction by ultrasonic vibrations.

This model is applicable to various cases of ultrasonic lubrication because it does not depend on the pattern of applying ultrasonic vibrations. It breaks the vibrations down into projections in three orthogonal directions and evaluates them separately.

3. Experiment

3.1. Set-up and schematics

A series of experiments is conducted to study the influence of ultrasonic vibrations on friction reduction. The experimental set-up is shown in Fig. 4; the waveguide and sliding block are illustrated in Fig. 5. Vibrations are generated by a commercial ultrasonic welder (Dukane 220) and transmitted to a horn-shaped waveguide. Dimensions of the waveguide are 127 mm by 61 mm by 25.4 mm. Other methods to generate the ultrasonic excitation could be used, for instance discrete piezoelectric stacks or magnetostrictive actuators. A block with a curved top surface slides underneath the horn, creating a line contact with the bottom surface of the waveguide. The block is given a speed of 5 mm/s.

Since they are based on Poisson effect, the vibrations on the surfaces of the waveguide consist of longitudinal and transverse projections, which theoretically conjugate into straight-line vibrations with angles to the horizontal plane. The angles vary with different positions on the x-axis. However, due to the propagation and reflection of the ultrasonic wave within the waveguide, vibrations follow elliptical loci instead of straight lines.

The ultrasonic lubrication effect is expected to be most effective around the center-line of the waveguide where the half-wavelength node is located [26]. Therefore, tests are conducted around that area involving different material combinations. Table 1 lists the details of each test group. A frame is built to generate normal loads through an aluminum block with a curved surface on the waveguide from the top. Load cells are employed to measure the normal and tangential forces.

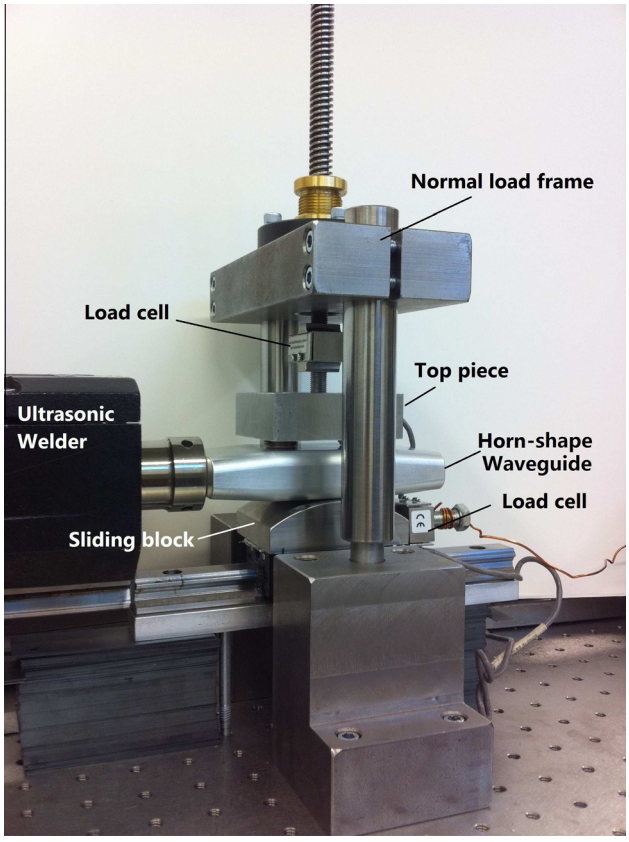

Fig. 4. Experimental set-up.

3.2. Ultrasonic vibrations

The longitudinal time-dependent displacement of the waveguide can be calculated as

$$u(x,t) = A\cos(2\pi ft)\sin(\pi x/L), \tag{16}$$

where L is the length of the waveguide, A is the amplitude of vibrations in the longitudinal direction, and f is the frequency of ultrasonic vibrations.

The vertical displacement can be calculated as

$$v(x,t) = B\cos(2\pi ft)\cos(\pi x/L), \tag{17}$$

where B is the amplitude of vibrations in the vertical direction.

Detailed derivation of (16) and (17) can be found in the appendix. To obtain the actual vibration amplitude A and B, a laser vibrometer is employed to measure vibration mode shapes and amplitudes. The amplitudes are listed in Table 1.

4. Results and discussion

4.1. Contact parameters

The parameters used in the cube model simulations are listed in Table 2. The surface roughness parameters R_q, R_s, and η are estimated using surface roughness comparison standards. These standards give prevalent surface roughness values for different surface finishes. The model simulation gives the same contact parameters for test 1 (aluminum waveguide with stainless steel block) and test 2 (stainless steel waveguide and aluminum block). Cube heights under different normal loads are calculated using elastic–plastic equations (Eqs. (4) and (5)) and plotted in Fig. 6. Cube heights calculated using elastic equations are also plotted in this figure for comparison. A similar comparison of real contact areas is shown in Fig. 7.

It is observed in Fig. 6 that the elastic–plastic assumption leads to a smaller cube height and associated smaller separation between surfaces. The elastic–plastic model predicts less separation between stainless steel surfaces than between aluminum and stainless steel, while the opposite is true for the purely elastic model. For the aluminum and stainless steel combination, at 40 N normal load, the separation is around 25 μm using the purely elastic model but 18 μm using the elastic–plastic model; the difference between the two models is around 7 μm under the range of normal loads considered. For the stainless steel and stainless steel combination, the discrepancy between the models is larger, close to 9 μm on average.

A smaller separation indicates a greater real contact area. When the first contacting asperities start to undergo plastic deformation, the plastic regions continue growing but contribute no additional resisting force. Therefore, as the normal force increases, more asperity contacts are formed and a larger real contact area is generated. As shown in Fig. 7, there is up to a sevenfold increase in contact area as the normal force varies over the range. The discrepancy between the elastic and elastic–plastic models is about 10^2 μm^2.

4.2. Friction

Friction forces at various normal loads obtained from all three test groups are plotted in Fig. 8, and the corresponding dynamic friction coefficients are plotted in Fig. 9. In different test groups, the normal loads adopted are different. As shown in the figures, test 1 uses 11 normal loads from 40 N to 240 N with an interval of 20 N. Due to the different test conditions, the other two groups

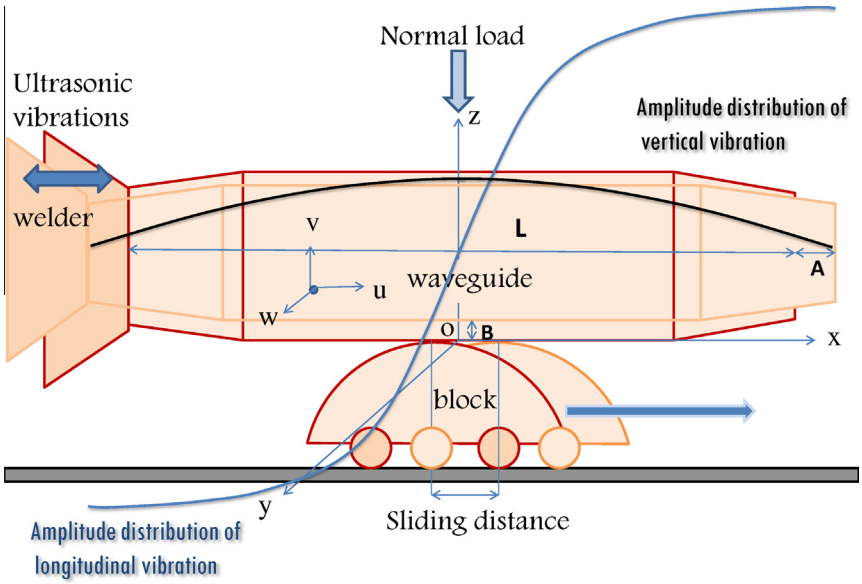

Fig. 5. Illustration of the waveguide and sliding block, showing the amplitude distribution of vertical and horizontal vibration in the waveguide.

Table 1
Test parameters.

Test	Materials[a]	A (μm)	B (μm)	Sliding distance (mm)
1	Al & SS	11.46	1.1	−6 to +6
2	SS & Al	10.52	1.05	+2.5 to +5
3	SS & SS	10.52	1.05	+2.5 to +5

[a] Al = aluminum, SS = stainless steel, in the order of waveguide and sliding block.

Table 2
Parameters used in model simulations.

Symbol	Parameter	Value	Unit
R_q	Asperity heights deviation	6	μm
R_s	Asperity summits radius	1.7	μm
A_n	Nominal contact area	1×10^{-4}	m^2
η	Areal asperity density	47×10^9	$/m^2$
E_1	Young's modulus of aluminum	73	GPa
ν_1	Poisson's ratio of Aluminum	0.33	–
E_2	Young's modulus of stainless steel	200	GPa
ν_2	Poisson's ratio of stainless steel	0.29	–
Y_0	Failure strength of the softer material	410	MPa

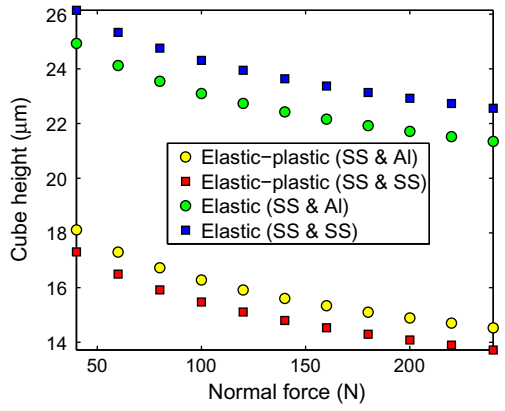

Fig. 6. Comparison of cube heights calculated from elastic and elastic–plastic models.

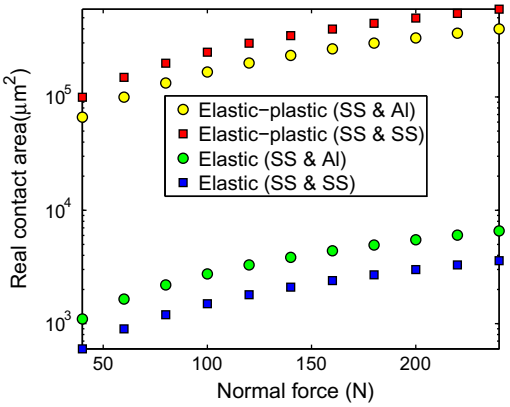

Fig. 7. Comparison of cube real contact area calculated from elastic and elastic–plastic models.

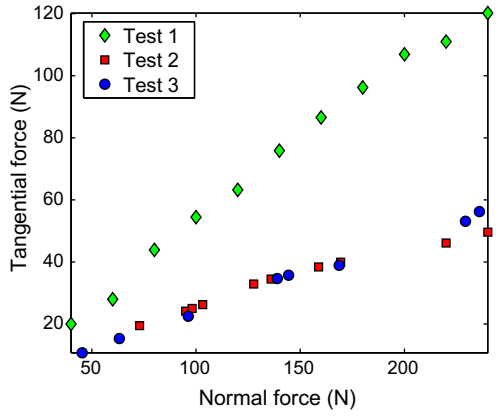

Fig. 8. Comparison of dynamic friction forces measured from tests.

use 10 and 8 normal loads, respectively, which cover the same range but without an even distribution of forces.

Results from all three test groups show good linearity between the normal loads and the tangential forces, which presents

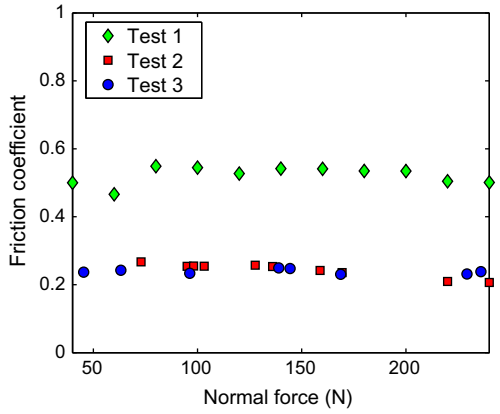

Fig. 9. Comparison of dynamic friction coefficients measured from tests.

relatively constant friction coefficients within the different groups. However, test 1 gives higher friction forces than test 2. The average coefficients are respectively 0.54 and 0.26. It is emphasized that those two test groups give different results even though they are from the same two types of materials. The different behavior may be caused by the way normal forces are applied onto the contact interface of the two materials. For the stainless steel waveguide (tests 2 and 3), the results show that the friction forces are approximately the same regardless of sliding block material.

4.3. Friction reduction

A comparison of test results and model simulations for all three test groups is shown in Fig. 10. Each figure plots three sets of data, two of which are from tests and one from model simulations. The red squares denote natural friction forces. The blue circles indicate friction forces with ultrasonic vibrations measured from tests. The green diamonds are friction forces with ultrasonic vibrations predicted by the cube model. The model parameters used for calculation are listed in Table 2.

All three sets of data show good linearity between friction forces and normal forces, which indicate constant dynamic friction coefficients. But in test 2, at three points when normal loads are larger than 160 N, reduced friction forces measure larger than the linearity indicates, which may be caused by experimental error.

Friction forces are substantially reduced in all three cases when ultrasonic vibrations are employed. The friction reduction percentage is defined as

$$p = \frac{F_t - F_t'}{F_t} \times 100. \tag{18}$$

Percentages from both tests and simulations are plotted in Fig. 11 for comparison.

Tests 1 and 2 have friction reduction in the range of 30–50% and show trends that higher normal loads provide lower reduction percentages. Test 3 has higher reduction percentage, in the range of 50–60%, but results show no evident decreasing trend when the normal load goes up.

Note that both the waveguide and sliding block used in test 3 are stainless steel, which is different from tests 1 and 2, which mix aluminum and stainless steel. Since stainless steel is harder than aluminum, it can be hypothesized that the harder the materials of the contacting surfaces, the higher the friction reduction. However, this hypothesis requires more testing using materials with a wider range of hardness.

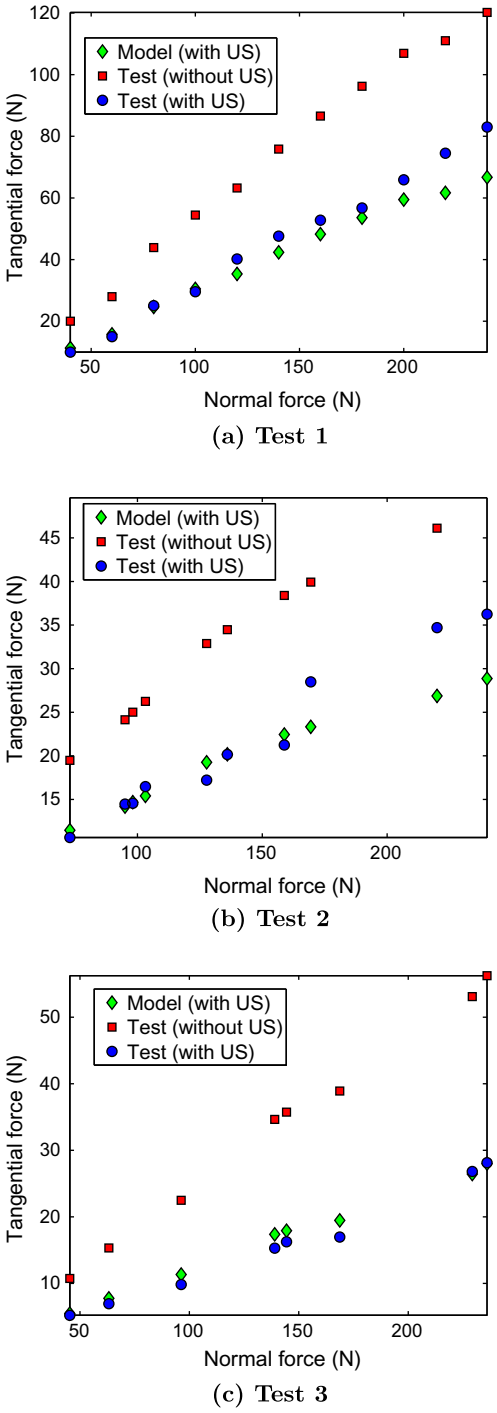

Fig. 10. Comparison of friction reduction between tests and model simulations.

Another observation is that test 3 reveals less wear than tests 1 and 2, which may also be explained by the fact that stainless steel is harder than aluminum. In tests 1 and 2, fretting wear mostly occurs on aluminum parts but much less on stainless steel parts.

4.4. Comparison of model simulation and tests

The results show that the model predictions closely match the experimental data. However, there are some discrepancies between the test and model, as seen in each figure. In tests 1 and 2, the discrepancy becomes evident when normal load is increased. Despite possible test errors, another reason for that could be the

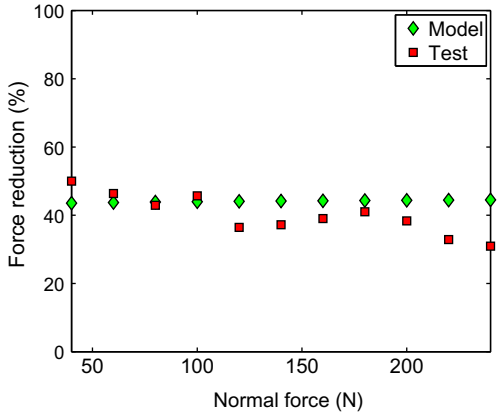

(a) Test1

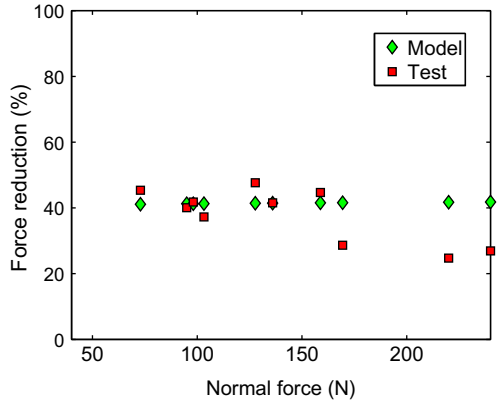

(b) Test2

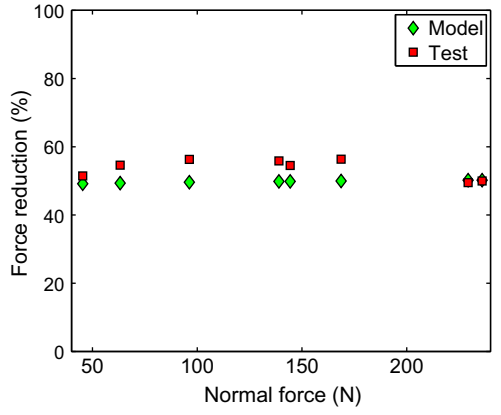

(c) Test3

Fig. 11. Comparison of friction reduction percentage between tests and model simulations.

asperity heights distribution model, an exponential function used to approximate the Gaussian distribution for ease of calculation. The discrepancy between those two functions becomes greater as normal loads increase.

The relative error between test and simulation is defined as

$$e = \frac{|\text{test} - \text{model}|}{\text{test}} \times 100. \tag{19}$$

Most errors from all three tests are below 20%, showing good agreement.

5. Conclusion and future work

In this work, an improved cube model is presented which describes ultrasonic lubrication under a range of conditions. Ultrasonic vibrations are projected on three orthogonal directions and the influence of each projection on friction reduction is calculated. An overall reduction result summarizes all three projections. The calculation of contact parameters takes into consideration plastic deformation, which gives smaller distances between two surfaces and larger real contact areas.

A series of experiments is designed and conducted to test ultrasonic lubrications under discrete normal loads from 40 N to 240 N. Results show positive reduction results for all three material combinations.

The cube model is used to describe the reduction in friction force using parameters from the tests and contact model. These simulations show good agreement with the test results, reflecting average relative errors below 20% despite the fact that small discrepancies exist with normal loads above 160 N. Future work may be able to address this issue by employing a Gaussian distribution for asperity heights instead of an exponential distribution.

Furthermore, the cube model can be applied to model dynamical systems with ultrasonic lubrication devices. The results are of great interest in predicting system outputs, thus aiding in system design. Through in-depth analysis of stress, strain and plastic deformations of asperities, the cube model may be used in modeling wear reduction.

Acknowledgments

Support for this research comes from the member organizations of the Smart Vehicle Concepts Center (www.SmartVehicleCenter.org), a National Science Foundation Industry/University Cooperative Research Center (I/UCRC).

Appendix A. Waveguide kinematics

Waveguide kinematics helps to understand the generation and propagation of ultrasonic vibrations in the waveguide. In this study, the influence of the tapering and rounded edges of the waveguide is neglected for simplicity, and the vibrations of the waveguide are treated as a superposition of the motion of all modes,

$$u(x,t) = \sum_{n=1}^{\infty} (a_n \sin \omega_n t + b_n \cos \omega_n t) U_n(x), \tag{A.1}$$

where ω_n is the nth order frequency and $U_n(x)$ is the function of the nth order normal mode shape, which has the form

$$U_n(x) = c_n \sin(\omega_n x/c_0) + d_n \cos(\omega_n x/c_0), \tag{A.2}$$

where c_0 is the axial speed of wave propagation. For each mode n, there exists a wave equation [26]

$$\frac{\partial^2 U_n}{\partial x^2} + \frac{{\omega_n}^2 U_n}{c_0^2} = 0. \tag{A.3}$$

It is deduced that $d_n = 0$; using the boundary conditions $\partial u(-L/2,t)/\partial x = 0$ and $\partial u(L/2,0)/\partial x = 0$, it is obtained that $\cos(\omega_n L/2c_0) = 0$, thus

$$\omega_n = n\pi c_0/L (n = 0, 1, 2 \ldots). \tag{A.4}$$

Given that the frequency and the waveguide length in this paper are respectively 20 kHz and 0.127 m, the order of the vibration, therefore, is equal to 1, which means that the vibration is at the half-wavelength frequency and its corresponding normal mode function can be written as

$$U_1 = c_1 \sin(\omega_1 x/c_0) = c_1 \sin(\pi x/L). \tag{A.5}$$

Thus, the longitudinal vibration function is written as

$$u(x,t) = b_1 \cos(2\pi f t) U_1 = b_1 c_1 \cos(2\pi f t) \sin(\pi x/L). \tag{A.6}$$

Letting $A = b_1 c_1$, the function of longitudinal displacement (16) is derived. The vertical strain is caused by longitudinal strain, known as Poisson's effect. The longitudinal strain is calculated as

$$\varepsilon_x = \frac{\partial u(x,t)}{\partial x} = \frac{A\pi}{L} \cos(2\pi f t) \cos(\pi x/L). \tag{A.7}$$

Therefore, the vertical strain is

$$\varepsilon_y = v\varepsilon_x = \frac{A\pi v}{L} \cos(2\pi f t) \cos(\pi x/L). \tag{A.8}$$

The vertical displacement of the point at the bottom surface of the waveguide is the integration of the strain over half of the thickness of the waveguide, which is expressed as

$$v(x,t) = \frac{DA\pi v}{2L} \cos(2\pi f t) \cos\left(\frac{\pi x}{L}\right), \tag{A.9}$$

where D is the thickness of the waveguide. Letting $B = DA\pi v/2L$, the function of vertical displacement (Eq. (17)) is derived. In this paper, the values of A and B are determined by Doppler laser vibrometer measurements.

References

[1] W.P. Mason, Physical Acoustics and the Properties of Solids, Van Nostrand, Princeton, New Jersey, 1958.
[2] R. Pohlman, E. Lehfeldt, Influence of ultrasonic vibration on metallic friction, Ultrasonics 4 (4) (1966) 178–185.
[3] W. Littmann, H. Storck, J. Wallaschek, Sliding friction in the presence of ultrasonic oscillations: superposition of longitudinal oscillations, Arch. Appl. Mech. 71 (2001) 549–554.
[4] H. Storck, W. Littmann, J. Wallaschek, M. Mracek, The effect of friction reduction in presence of ultrasonic vibrations and its relevance to travelling wave ultrasonic motors, Ultrasonics 40 (2002) 379–383.
[5] V.C. Kumar, I.M. Hutchings, Reduction of the sliding friction of metals by the application of longitudinal or transverse ultrasonic vibration, Tribol. Int. 37 (8) (2004) 833–840.
[6] V.L. Popov, J. Starcevic, A.E. Filippov, Influence of ultrasonic in-plane oscillations on static and sliding friction and intrinsic length scale of dry friction processes, Tribol. Lett. 39 (2010) 25–30.
[7] S. Dong, M.J. Dapino, Piezoelectrically-induced ultrasonic lubrication by way of Poisson effect, Proc. SPIE 8343 (2012) 83430L.
[8] S. Bharadwaj, M.J. Dapino, Friction control in automotive seat belt systems by piezoelectrically generated ultrasonic vibrations, Proc. SPIE 7645 (2010) 76450E.
[9] S. Bharadwaj, M.J. Dapino, Characterization of friction reduction with tangential ultrasonic vibrations using a SDOF model, Int. J. Vehicle Des. 63 (2/3) (2013).
[10] V.P. Severdenko, V.V. Klubovich, A.V. Stepanenko, Ultrasonic Rolling and Drawing of Metals, Consultants Bureau Publisher, New York, 1972.
[11] K. Cunefare, N. Montburn, V. Rastelli, J. Aller, M. Dzirasa, Burst mode dither control of automotive brake squeal, J. Acoust. Soc. Am. 109 (5) (2001) 2369.
[12] K. Cunefare, A. Graf, Experimental active control of automotive disc brake rotor squeal using dither, J. Sound Vibrat. 250 (4) (2002) 579–590.
[13] A. Pasierb, A. Wojnar, An experimental investigation of deep drawing and drawing processes of thin-walled products with utilization of ultrasonic vibrations, J. Mater. Sci. Technol. 34 (1992) 489–494.
[14] Y. Ashida, H. Aoyama, Press forming using ultrasonic vibration, J. Mater. Sci. Technol. 187–188 (2007) 118–122.
[15] M. Hayashi, M. Jin, S. Thipprakmas, M. Murakawa, J.C. Hung, Y.C. Tsai, C.H. Hung, Simulation of ultrasonic-vibration drawing using the finite element method (FEM), J. Mater. Sci. Technol. 140 (2003) 30–35.
[16] N. Hatanaka, K. Yamaguchi, N. Takakura, Finite element simulation of the shearing mechanism in the blanking of sheet metal, J. Mater. Sci. Technol. 139 (2003) 64–70.
[17] W. Yeh, T. Chu, S. Wang, K. Fuh, K. Chen, Finite element analysis of blanking process by superimposing ultrasonic vibrations, Adv. Mater. Res. 201–203 (2011) 126–132.
[18] B. Bhushan, Introduction to Tribology, John Wiley & Sons, New York, 2002.
[19] J.A. Greenwood, J.B. Williamson, Contact of nominally flat surfaces, Proc. R. Soc. Am. 295 (1966) 300–319.
[20] D. Cohen, Y. Klingerman, I. Etsion, A model for contact and static friction of nominally flat rough surfaces under full stick contact condition, J. Tribol. 130 (031401) (2008) 1–9.
[21] A.A. Polycarpou, I. Etsion, Analytical approximations in modeling contacting rough surfaces, ASME J. Tribol. 121 (1999) 234–239.
[22] W.R. Chang, I. Etsion, D.B. Bogy, An elastic–plastic model for the contact of rough surfaces, ASME J. Tribol. 109 (1987) 257–263.
[23] R.C. Craig, Mechanics of Materials, John Wiley & Sons, New York, 2000.
[24] W.P. Mason, K.J. Marfurt, D.N. Beshers, J.T. Kuo, Internal friction in rocks, J. Acoust. Soc. Am. 63 (5) (1978) 1596–1603.
[25] P. Dahl, A Solid Friction Model, Aerospace Corp, 1968.
[26] K.F. Graff, Wave Motion in Elastic Solids, Clarendon Press, Oxford, 1975.